Carbonaceous aerosols on the south edge of the Tibetan Plateau: concentrations, seasonality and sources

Z. Cong[1, 3, 5], S. Kang[2, 5], K. Kawamura[3], B. Liu[1], X. Wan[1], Z. Wang[1], S. Gao[1], P. Fu[4]

[1]{Institute of Tibetan Plateau Research, CAS, Beijing 100101, China}
[2]{State Key Laboratory of Cryospheric Sciences, CAS, Lanzhou 730000, China}
[3]{Institute of Low Temperature Science, Hokkaido University, Sapporo, 060-0819, Japan}
[4]{LAPC, Institute of Atmospheric Physics, CAS, Beijing 100029, China}
[5]{CAS Center for Excellence in Tibetan Plateau Earth Sciences, Beijing 100101, China}

Correspondence to
S. Kang (shichang.kang@itpcas.ac.cn)
K. Kawamura (kawamura@lowtem.hokudai.ac.jp)

Abstract

To quantitatively evaluate the effect of carbonaceous aerosols on the south edge of the Tibetan Plateau, aerosol samples were collected weekly from August 2009 to July 2010 at Mt. Everest (QOMS, 28.36°N, 86.95°E, 4276 m a.s.l.). The average concentrations of OC, EC and WSOC were 1.43, 0.25 and 0.77 μg m^{-3}, respectively. The concentration levels of OC and EC at QOMS are comparable to those at high elevation sites on the southern slopes of the Himalayas (Langtang and NCO-P), but three to six times lower than those at Manora Peak, India and Godavari, Nepal. Sulfate was the most abundant anion species followed by nitrate, accounting for 25% and 12% of total ionic mass, respectively. Ca^{2+} was the most abundant cation species (annual average of 0.88 μg m^{-3}). The dust loading, represented by Ca^{2+} concentration, was relatively constant throughout the year. OC, EC and other ionic species (NH_4^+, K^+, NO_3^-, and SO_4^{2-}) exhibited a pronounced peak in the pre-monsoon period and a minimum in the monsoon season, being similar to the seasonal trends of aerosol composition reported previously from the southern slope of the Himalayas, such as Langtang and NCO-P. The strong correlation of OC and EC in QOMS aerosols with K^+ and levoglucosan indicates that they were mainly originated from biomass burning. The fire spots observed by MODIS and their backward trajectories further demonstrate that in pre-monsoon season, agricultural and forest fires in the northern India and Nepal were most likely sources of carbonaceous aerosol at QOMS. Moreover, the CALIOP observations confirmed that air pollution plumes crossed the Himalayas during this period. The highly coherent variation of daily aerosol optical depth (AOD, 500 nm) between QOMS and NCO-P indicates that both slopes of the Himalayas share a common atmospheric environment regime. In addition to large-scale atmospheric circulation, the unique mountain/valley breeze system can also have an important effect on air pollutant transport.

1 Introduction

The Tibetan Plateau (TP) and the surrounding Hindu Kush-Himalayan mountains are known as the "Third Pole" of the Earth (Qiu, 2008), due to its immense area and high elevation (Yao et al., 2012). Because of the contrast of thermal heating between continent and ocean, the TP plays a fundamental role in the formation of the Asian monsoon system and Northern Hemispheric climatology (Wu and Zhang, 1998). The TP and Himalayas, with more than 100,000 km^2 of glaciers, contain the largest ice mass outside the Polar region (Xu et al., 2009;Yao et al., 2012). Over the past decades, climate change impacts have been revealed due to marked air temperature rising and dramatic glacier shrinkage across this area (Kang et al., 2010).

Due to sparse human population and minimal industrial activities, the TP is considered one of the most pristine terrestrial regions, alongside the Arctic and Antarctic. However, growing evidence has demonstrated that widespread atmospheric brown clouds (ABCs) over South Asia may affect this region (Bonasoni et al., 2010;Kaspari et al., 2011;Lu et al., 2012;Xia et al., 2011;Wang et al., 2010). Research has attempted to reveal a link between climate change over the TP (e.g. air temperature rising, glacier melting) and the distribution of anthropogenic pollutants (mainly absorbing carbonaceous materials) (Qian et al., 2015;Wang et al., 2014b). Ramanathan and Carmichael (2008) reported that in the high Himalayan region, solar heating caused by black carbon (BC) could be approximately equivalent to the warming by CO_2 in terms of the melting of snowpack and glaciers.

Could we quantitatively differentiate the various factors that contribute to glacier melting, including aerosols, greenhouse gas, and BC deposition on the snow surface? Clearly, to answer this question and reduce the uncertainties, adequate knowledge of the aerosol properties is urgently needed. Some scientists have used different models to reveal the importance of carbonaceous aerosol in this region (Menon et al., 2010;Qian et al., 2011;Yasunari et al., 2010). So far, most works on aerosol composition have been carried out on the south slope of the Himalayas, such as Langtang, Nepal (Carrico et al., 2003), Godavari (Stone et al., 2010), Nepal Climate

Observatory-Pyramid (NCO-P) (Decesari et al., 2010) and Manora Peak, India (Ram et al., 2010). Long-term aerosol chemistry measurements from the TP are extremely scarce mainly due to its remoteness and challenging weather conditions, with measurements limited to Lulang (Zhao et al., 2013), Waliguan (Ma et al., 2003), Nam Co (Ming et al., 2010) and Qinghai Lake (Li et al., 2013). As we know, no systematic data on carbonaceous aerosols from the south edge of the TP (i.e. the north slope of Himalayas) has been reported. From the spatial distribution of aerosols observed by satellites (e.g. MODIS, Fig. S1), there was a clear difference between South Asia and Tibetan Plateau. Therefore, as the boundary area this region merits special attention.

In this paper, we present results from one-year measurements of organic carbon (OC), elemental carbon (EC), water-soluble organic carbon (WSOC) and major ions in the aerosols at Mt. Everest, the south edge of the TP. Our aim is to provide baseline levels of aerosols for this region, reduce the assessment uncertainties of aerosol radiative forcing and provide more information on their transport mechanism.

2 Methodology

2.1 Description of research site

In 2005, Qomolangma (Mt. Everest) Station for Atmospheric and Environmental Observation and Research (briefly QOMS, 28.36°N, 86.95°E, 4276 m a.s.l.) (Fig. 1) was established to begin continuous monitoring of the environment (Ma et al., 2011). A solar electricity system generates the power to maintain the instrumentation. According to the observations achieved so far, the Mt. Everest region (QOMS) is a typical representative of the middle Himalayas in terms of climate, air circulation systems and environmental characteristics (Chen et al., 2012;Li et al., 2012;Ma et al., 2011). Sandy soil with sparse grass and small rocks cover the land surface around the QOMS. Due to its harsh environment, QOMS is relatively isolated from industrial zone and cities, with a very limited local population (Ma et al., 2011).

2.2 Aerosol sampling

From August 2009 to July 2010, total suspended aerosol particle (TSP) samples were collected weekly at QOMS using medium-volume samplers (KC-120H, Laoshan Co., flow rate: 100 L min^{-1} at standard condition). The sampling duration of each sample was 24 hours. Aerosols were collected using 90-mm diameter quartz filters (QM/A, Whatman, UK), which were pre-combusted at 450 °C for 6 hours. Field blanks were collected every month by placing filters into the filter holder for a few minutes with no air flowing. After sampling, the filters were wrapped with aluminum foil and frozen until analysis. Eventually, fifty samples were successfully obtained.

2.3 OC and EC analysis

The quartz filters were analyzed for OC and EC using a carbon analyzer (DRI model 2001). Briefly, a filter aliquot (0.5 cm^2) was analyzed for eight carbon fractions following the IMPROVE-A thermal/optical reflectance (TOR) protocol (Cao et al., 2007;Chow et al., 2007). Four OC fractions (OC1, OC2, OC3 and OC4) were determined at 140, 280, 480 and 580 °C in pure He atmosphere, which was subsequently switched to 2% O_2/98% He atmosphere to determine EC1, EC2 and EC3 at 580, 740 and 840 °C, respectively. The residence time of each heating step was defined by the flattening of the carbon signal. The pyrolyzed carbon fraction (OPC) is determined when reflected laser light returns to its initial value after oxygen is introduced. In general, OC is defined as OC1 + OC2 + OC3 + OC4 + OPC and EC is defined as EC1 + EC2 + EC3 - OPC. The detection limit for the carbon analyzer was 0.05 μgC cm^{-2} for OC and 0.05 μg C cm^{-2} for EC.

2.4 Water-soluble ions and WSOC

An aliquot of filter (2.54 cm^2) was extracted with 10 ml ultrapure water with sonication for 30 minutes. The extracted solutions were filtrated with syringe-driven filters (Millex-GV PVDF, 0.22 μm; Millipore, Ireland) to remove the quartz fiber debris and other insoluble impurities. Then the water-soluble ionic species (Cl^-, SO_4^{2-}, NO_3^-, Ca^{2+}, Na^+, K^+, Mg^{2+} and NH_4^+) were analyzed using an ion chromatograph (761

Compact IC, Metrohm). Anions were measured with a suppressor on a Shodex SI-90 4E column using an eluent mixture of 1.8 mM Na_2CO_3, 1.7 mM $NaHCO_3$ and 40 mM H_2SO_4 at a flow rate of 1.2 mL min^{-1}. Cations were determined on a Metrohm C2-150 column with tartaric acid (4 mM) and dipicolinic acid (1 mM) as an eluent. The overall uncertainty in determining ionic species is less than 4% (Miyazaki et al., 2010). The detection limit for cations and anions was 0.01 μg m^{-3}, which was calculated according to the air volume of actual samples.

To quantify WSOC, a portion of filter (19.1 cm^2) was extracted and filtrated using the same procedure for major ions described above. Then the extract was injected into a total carbon analyzer (TOC-V, Shimadzu). The method detection limit (MDL) used was 4 μg L^{-1} with a precision of ±5%. All the concentrations of carbonaceous and ionic components in this study are field-blank corrected. It should be noted that there are possible sampling artifacts by the adsorption/evaporation of gaseous organic materials on/from the quartz membrane. However, no quantitative information on such positive/negative artifact is available in this study, therefore, no correction was made for the data of carbonaceous components.

2.5 Determination of levoglucosan

Levoglucosan was determined by GC/MS after the extraction of the samples with a methanol/methylene chloride mixture followed by BSTFA derivatization. Details of the analytical procedure is presented elsewhere (Fu et al., 2008).

2.6 Meteorology and backward air mass trajectories

At the QOMS station, various meteorological parameters (Fig. 2) were recorded by a 40 m atmospheric boundary layer tower that measures wind speeds, wind direction (014A-L, Met One), relative humidity, air temperature, air pressure (HMP45C, Vaisala) and rain intensity (TE525MM-L, Young) (Chen et al., 2012;Li et al., 2012). Monthly mean air temperature reaches a maximum of 12.3°C in July, with a minimum in January of -3.2°C. Humidity is highest in August while lowest in December. Precipitation was unevenly distributed throughout the year, with more

than 90% of annual precipitation occurring from June to September. According to the meteorological parameters at QOMS (Fig. 2), the climatology is roughly divided into four seasons, i.e. pre-monsoon, monsoon, post-monsoon and winter (The definition of different seasons was shown in Table S1). These seasons are generally in agreement with the seasonal definition made in a previous study in this region (Bonasoni et al., 2010). In general, this region is controlled by Indian Monsoon system in summer (June-August), characterized by relatively high temperature and humid weather with prevailing southerly winds. While in the remaining period, westerlies dominate the large-scale atmospheric circulation patterns with limited precipitation.

To reveal the transport pathway of air masses that arrive at QOMS, seven-day backward trajectories were computed using the HYSPLIT model (Draxler and Rolph, 2012) and GDAS (Global Data Assimilation System) data for each sampling day. Given the typical height of the planetary boundary layer (PBL) in this region (Chen et al., 2012), the arrival height of air mass in these modeling was set to 500 m above ground level.

3 Results and discussion

3.1 Characteristics and temporal variations of OC and EC

The statistical summaries of carbonaceous components in the aerosols from QOMS are presented in Table 1. The average concentrations of OC and EC in the aerosols from QOMS were 1.43 ± 1.16 and 0.25 ± 0.22 μg m^{-3}, respectively. The concentration levels of OC and EC at QOMS are about three times higher than those of Muztagh Ata, northwest TP (Cao et al., 2009), while they are comparable to those reported from the Central and Northeastern TP (Li et al., 2013;Ming et al., 2010) (Table 2). In contrast, OC and EC concentrations from the southeastern TP (Tengchong and Lulang) are significantly higher than those at QOMS, possibly due to the higher contribution of biomass burning (Engling et al., 2011;Zhao et al., 2013). When compared with sites on the south slopes of the Himalayas, QOMS data present the same order of OC

and EC with NCO-P (Decesari et al., 2010) and Langtang (Carrico et al., 2003), but three to six-fold lower than Manora Peak, India (Ram et al., 2010) and Godavari, Nepal (Stone et al., 2010). The latter two sites are at lower altitudes and are closer to the populated areas of South Asia, heavily influenced by anthropogenic emission. Generally, the high altitude sites on both sides of the Himalayas (i.e. Langtang, NCO-P and QOMS) exhibit similar OC and EC abundance, which could be considered as a regional baseline level to be used in the regional climate model as input parameters.

In a previous study, Ming et al. (2008) estimated atmospheric EC concentration in the region based on the analysis of an ice core from the East Rongbuk Glacier, Mt. Everest. Apparently, there is a big discrepancy between our EC data (annual average of 0.25 ± 0.22 μg m^{-3}) and the EC data estimated by ice cores (average: 0.077 ± 0.045 μg m^{-3} during 1951–2001). One potential reason is that several parameters (e.g. scavenging ratio of EC) need to be assumed to convert the EC in the ice core to atmospheric concentration, which may introduce some uncertainty. Moreover, dramatically increasing trends of EC in the Himalayas and the TP ice cores have been reported (Cong et al., 2013;Kaspari et al., 2011), i.e. a two and a half to three fold rise in recent decades compared to background conditions. Therefore, our EC data for 2009–2010, which is higher than the average EC concentration for 1951–2001, is reasonable.

The OC/EC ratios at QOMS range from 1.91 to 43.8, with average of 6.69. Such high ratios are commonly found in different areas of the TP (Table 2). There are two potential reasons for those high OC/EC ratios. One reason may be a strong solar radiation (exceeding 7500 MJ m^{-2}) over the TP, because substantial secondary organic carbon (SOC) could be formed through photochemical reaction (Wan et al., 2015). The other potential reason is the influence of biomass burning. Usually, the aerosols emitted from biomass burning have higher OC/EC ratio. For example, Watson et al. (2001) have reported an OC/EC ratio of 14.5 for forest fires. Considering the specific condition of this study (QOMS), the second reason is more likely, i. e. the strong

influence of biomass-burning emissions. The higher abundance of OC than EC on the TP emphasizes that OC should not be ignored in the quantification of total radiative forcing of aerosol by climate models (Kopacz et al., 2011). Although some organic carbon has light-absorbing capability (i.e. brown carbon), the net effect of organic carbon on climate is negative (cooling) (Stocker et al., 2013), which may attenuate the positive radiative forcing caused by EC.

The temporal variations of the aerosol OC, EC and WSOC are illustrated in Fig. 3. Clearly, the OC, EC and WSOC share a significant seasonal pattern，i.e. a maximum in the pre-monsoon period and a minimum in the monsoon season. Higher abundance of OC and EC imply that the contributions from anthropogenic activities are larger in pre-monsoon than other seasons. Similar seasonal trends of aerosol composition were also reported previously on the south slopes of the Himalayas, such as Langtang (Carrico et al., 2003) and NCO-P (Decesari et al., 2010). This phenomenon indicates that these regions (Mt. Everest), both slopes of the Himalayas, have a common atmospheric environmental regime, although the high altitude of the Himalayas was once considered a good barrier for the spreading of atmospheric pollutants in South Asia. This point will be further discussed in Section 3.5.

3.2 Relationship between OC and EC

Examining the relationship between OC and EC can provide meaningful insights into the origin and possible reaction process during the transport of carbonaceous aerosols (Turpin and Huntzicker, 1995). At QOMS, a strong correlation (R^2 = 0.81) was observed between OC and EC during the pre-monsoon season (Fig. 4a), indicating common emission sources and transport processes. The correlation coefficients between OC and EC in the other three seasons were lower than that of the pre-monsoon season (Fig. 4b, c, d), with the lowest correlation observed in the summer monsoon season (R^2 = 0.08), suggesting that there are other influences. In addition to the common emission sources (e.g. fossil fuel and biomass burning), OC could also be produced by biogenic sources and the formation of secondary OC (SOC). The relative importance of different sources and/or formation process merits a

further study.

SOC has often been calculated from the primary OC/EC ratio (EC-tracer method) (OC_{pri} = EC*$(OC/EC)_{min}$, OC_{sec} = OC_{tot} – OC_{pri}), which is assumed to be relatively constant for a given site (Turpin and Huntzicker, 1995). The lowest OC/EC ratio in the aerosol was suggested for use as the primary source to calculate the SOC abundance (Castro et al., 1999), when the secondary production of OC is expected to be minimal. However, for the samples from QOMS, we found that calculating SOC formation using this method was not reliable. The minimum OC/EC ratios differ greatly among various seasons (3.40, 3.78, 1.91 and 2.67 for pre-monsoon, monsoon, post-monsoon and winter, respectively). Even for each season (11–13 samples for each seasons), the lowest three values of OC/EC ratios also varied substantially. Therefore, the SOC formation estimated by the conventional EC-tracer method is not presented here.

3.3 Water-Soluble Organic Carbon (WSOC)

The WSOC in aerosols, a major proportion of total organic carbon, could affect the hygroscopic property of the particles and their ability to act as cloud condensation nuclei (CCN) (Psichoudaki and Pandis, 2013). The abundance of WSOC relative to OC could be employed as an indictor to decipher whether organic aerosol is primary or secondary, because SOC usually tends to be more water-soluble than primary organic matter (Psichoudaki and Pandis, 2013). The concentration of WSOC at QOMS varied from 0.07 to 3.22 μg m^{-3}, with an average of 0.77 μg m^{-3} (Table 1). The average WSOC/OC ratios at QOMS were 0.47, 0.59, 0.62 and 0.57 for pre-monsoon, monsoon, post-monsoon and winter, respectively. The lowest WSOC/OC in pre-monsoon indicated the dominant contribution from primary emission sources with poor aging and less SOA formation. Furthermore, in the pre-monsoon season, the WSOC concentration exhibited a significant positive correlation with OC (y = 0.54x-0.12, R^2 = 0.94), which could be ascribed to the influence of biomass combustion. Previous studies have revealed that organic matters emitted from biomass burning were substantially composed of water-soluble polar organic

compounds, including dicarboxylic acids, sugars, aromatic acids, etc. (Claeys et al., 2010;Fu et al., 2012;Kundu et al., 2010). No evident correlation was found between WSOC and OC in other seasons when OC concentrations were low (Fig. 5).

3.4 Water-Soluble Ionic Species (WSIS)

Sulfate was the most abundant anion species followed by nitrate, accounting for 25% and 12% of total ionic mass, respectively (Table 1). Ca^{2+} was the most abundant cation species with annual average of 0.88 μg m^{-3}. Cl^- and Na^+ only consisted of a very minor portion of total ions, indicating that at QOMS the influence of sea salt is negligible. Water-soluble Ca^{2+} is a typical tracer of crustal material (dust) (Ram et al., 2010). At QOMS, the time-series of Ca^{2+} was somewhat uniform throughout the years (Fig. 6), implying that the mineral dust loading at QOMS is relatively constant. This pattern was obviously in contrast to other ionic species (NH_4^+, K^+, NO_3^-, and SO_4^{2-}). The temporal variation patterns of Ca^{2+} and SO_4^{2-} are different (Fig. 6), and thus the correlation is not strong (R^2 = 0.27), which excludes the possibility that they predominantly co-occurred in some minerals (e.g. gypsum).

Soluble potassium (K^+) is a good tracer of biomass burning (Andreae and Merlet, 2001;Cachier et al., 1995). In our study, the K^+ concentrations were below detection limit in most samples, but K^+ concentrations did show peaks in pre-monsoon season (Fig. 6). Furthermore, K^+ and EC demonstrated a good relationship (R^2 = 0.66, n = 9) during that period, indicating that they were both derived from biomass burning (Fig. 7c). A significant correlation between NO_3^- and SO_4^{2-} was not surprising (Fig. 7a), because they generally form from the oxidation of NOx and SO_2, which are closely related to fossil fuel combustion. In the pre-monsoon season with a high abundance of NH_4^+ (Fig. 6), NH_4^+ and NO_3^- exhibited a good correlation (R^2 = 0.80, n = 9), implying that they are present as NH_4NO_3 in the aerosol particles.

The seasonal variation of biomass burning (K^+) coincided with that of ions associated with the fossil fuel combustion (NH_4^+, NO_3^-, and SO_4^{2-}), suggesting that in the pre-monsoon season, QOMS might have received mixed anthropogenic pollution. But another explanation is more plausible. According to earlier observation by

transmission electron microscopy (Li et al., 2003), large amounts of K_2SO_4 and KNO_3 were present in aged smoke aerosols from biomass burning. Andreae et al. (1988) pointed out that haze aerosol from biomass burning is comprised of abundant NH_4^+, K^+, NO_3^- and SO_4^{2-}. Similarly, NH_4^+, K^+, NO_3^- and SO_4^{2-} are also reported as major water-soluble inorganic ions in aerosols from biomass burning on the southeastern Tibetan Plateau (Engling et al., 2011). In addition to K^+, levoglucosan is also used as a specific marker for biomass burning, which is formed by the pyrolysis of cellulose but not formed by fossil fuel combustions (Simoneit et al., 1999). In the pre-monsoon season, EC, OC and K^+ show good correlations with levoglucosan (Fig. 8), which further indicate that carbonaceous components in QOMS aerosols were predominantly from biomass burning.

3.5 Transport mechanism of aerosols

Seven-day backward air mass trajectories corresponding to each sampling date were calculated using the Hysplit model (Draxler and Rolph, 2012). Seven days were chosen because of the typical residence time of carbonaceous aerosols in atmosphere. The trajectories were generally consistent with other descriptions of air circulation patterns in previous studies (Cong et al., 2009), which correspond to the South Asian monsoon regime (Fig. 9). In the summer monsoon season, air masses are derived from Bangladesh and northeast India, and bring moisture that originates in the Bay of Bengal. In the non-monsoon season, strong westerlies pass through western Nepal, northwest India, and Pakistan (i.e. Southern Himalayas). Although the transport pathways of air masses arriving at QOMS during pre-monsoon, post-monsoon and winter are similar (Fig. 9), a distinctly higher carbonaceous aerosol level was found only in the pre-monsoon season (Fig. 3), which emphasizes the importance of source strength changes.

According to the previous ABC research (Ramanathan et al., 2005) and the emission inventory (Wang et al., 2014a), a high loading of atmospheric pollutants exists over the southern slopes of the Himalayas, which was pronounced in the pre-monsoon season. We further checked the biomass burning emission from different seasons

using the active fire product from MODIS (MODerate-resolution Imaging Spectroradiometer, both Terra and Aqua dataset), which was provided by Fire Information for Resource Management System (FIRMS, https://earthdata.nasa.gov/firms). Figure 10 clearly shows that the active fire counts (representing the agricultural burning and forest fires) peaked in pre-monsoon (April). This finding is in agreement with the vegetation fire study on the southern slopes of the Himalayas by Vadrevu et al. (2012). In general, the seasonal pattern of carbonaceous components (OC, EC and WSOC), their strong correlation with K^+ and levoglucosan, together with the air mass trajectories and active fire spots distribution, all suggest that the higher loadings of carbonaceous aerosols in the pre-monsoon season at QOMS were most likely affected by the biomass burning (agricultural and forest fires) in northern India and Nepal.

In addition to the large-scale atmospheric circulation, the local orographic effect on air pollutant transport should also be taken into account (Hindman and Upadhyay, 2002). In mountainous areas, because of the temperature difference between mountaintop and lowland, a diurnal valley wind system occurs that blows upward during the day and reverses into downward during the night. As shown by Bonasoni et al. (2010), the wind regime at NCO-P (southern slope of the Himalayas) was characterized by an evident daily circle of mountain/valley breeze. During the daytime, the valley winds (southerly) were predominant with maximum wind speed in the afternoon. Therefore, the daytime up-valley breeze delivered the air pollutants from the foothills (South Asia ABC) to higher altitudes (>5000 m a.s.l.). Aerosol mass concentration, BC and ozone at NCO-P exhibit strong diurnal cycles, with minima during the night and maxima during the afternoon especially in the pre-monsoon season (Decesari et al., 2010;Marinoni et al., 2010). However, distinct mountain-valley breeze circulation was observed on the northern slopes of the Himalayas (QOMS). A dominating down-valley wind occurs on the north side of Mt. Everest in the daytime, especially in the afternoon. Further, the driving force of the vast snow cover at high altitude could form a “glacier wind”, and the up-valley air

362 flow produced by intense ground surface heating is overcome by down-valley air flow
363 “glacier wind” and “mountain wind” (Chen et al., 2012;Zou et al., 2008). Therefore,
364 daytime intense valley wind circulation could make the valleys efficient channels for
365 the transport of air pollutants crossing over the Himalayas (Fig. S2), i.e., from the low
366 altitude of South Asia to the Tibetan Plateau.

367 Because both QOMS and NCO-P have sun-photometers and participated in the
368 AERONET project, the same instrument (Cimel 318), the same data processing
369 method and simultaneous observation between QOMS and NCO-P make it possible to
370 compare AOD data directly between the two slopes of Himalayas (Xu et al.,
371 2014;Gobbi et al., 2010). As shown in Figure 11, the daily AOD (500 nm) of QOMS
372 and NCO-P varied in highly similar pattern (The correlation significant at $p<0.001$),
373 which suggesting that the observation at QOMS can also capture the pollution signals
374 as NCO-P. Recently, Lüthi et al. (2014) investigated the transport mechanisms of
375 pollutants across Himalayas using a high-resolution model. They found some
376 trajectories with low altitudes originate from the TP, and then flow down through
377 valleys to the foothills of Himalayas during nighttime where they can mix with air
378 pollutants, and are then blown onto the TP again during daytime. For the vertical
379 distribution of aerosols, two examples of such transport episode revealed by CALIOP
380 satellite now were provided in the Supplementary Information (Fig. S3), which
381 clearly showed the pollution plumes from South Asia could transport across
382 Himalayas during the pre-monsoon season.

383 We roughly estimated the timescale for air masses transported from the southern slope
384 of Mt. Everest (NCO-P) to QOMS. The straight distance between the two sites is
385 about 40 km, and along the valley the real distance is about 50 km if we consider the
386 terrain effect (Fig. 1). The average wind speed in pre-monsoon season is 7.86 m/s
387 (Table S1). This means that the air mass could travel from the southern slope of Mt.
388 Everest and reach QOMS in less than two hours, even at the average wind speed.
389 These results demonstrate that at QOMS we can capture the air pollution signal from
390 the southern Himalayas. This air mass transport of pollutants caused by mountain

terrain along the valley was also supported by WRF modeling, i.e. at the upper valley there is a pronounced southerly flow onto the Tibetan Plateau (Bonasoni et al., 2010). In this study, a similar seasonal trend of aerosol composition was revealed between the southern and northern slopes of the Himalayas. The most probable explanation is that the local mountain/valley breeze circulation (south-to north air flow) acts as the connection for the air pollutants crossing the Himalayas.

4 Summary and conclusions

A comprehensive knowledge of aerosol chemistry is crucial for assessing anthropogenic influences and evaluating the effect of radiative forcing. This research presents the first dataset of carbonaceous aerosols for the south edge of the Tibetan Plateau. The average concentrations of OC and EC in the aerosols at QOMS were 1.43 and 0.25 μg m^{-3}, with a standard deviation of 1.16 and 0.22 μg m^{-3}, respectively. The high altitude sites from both sides of the Himalayas (i.e. Langtang, NCO-P and QOMS) exhibit similar OC and EC abundances, which could be considered as a regional baseline level to be used as input parameters in the regional climate model. The most striking finding in this study is that carbonaceous components (OC, EC and WSOC) and several ionic species (NH_4^+, K^+, NO_3^- and SO_4^{2-}) exhibit a clear seasonal pattern with concentration maxima in the pre-monsoon season (March, April and May). A strong correlation (R^2 = 0.81) was observed between OC and EC during the pre-monsoon season, indicating their common emission sources and transport process. The EC and OC show good correlations with biomass burning tracers (K^+ and levoglucosan), which further suggests that carbonaceous components in QOMS aerosols mainly originate from biomass burning. Based on the active fire spots observed by MODIS and backward trajectories, we found that in pre-monsoon, agricultural and forest fires in northern India and Nepal are the most likely sources of carbonaceous aerosol at QOMS. In addition to large-scale atmospheric circulation (South Asia monsoon system and westerlies), local mountain wind systems can also play an important role. The south-to-north airflow along mountain valleys in the

Himalayas could closely connect the atmospheric environment between the two sides of the Himalayas. A higher time resolution research (diurnal) is imperative in the future to deepen our understanding of such important processes.

Acknowledgements

This study is supported by the NSFC (41075089, 41271073 and 41225002), Strategic Priority Research Program-Climate Change: Carbon Budget and Relevant Issues (XDA05100105), CAS, and partly by the Japan Society for the Promotion of Science (Grant-in-Aid No. 24221001). P. Fu appreciates the financial support from the "One Hundred Talents" program of the CAS. Z. Cong acknowledges the support of Youth Innovation Promotion Association. We thank B. Holben, G. Gobbi and other team member for their effort in maintaining AERONET sites (EVK2-CNR and QOMS/CAS). We would like to thank the NOAA Air Resources Laboratory team for providing the HYSPLIT-4 trajectory model. The CALIOP data were available from the Atmospheric Science Data Center.

References

Andreae, M. O., Browell, E. V., Garstang, M., Gregory, G., Harriss, R., Hill, G., Jacob, D., Pereira, M., Sachse, G., and Setzer, A.: Biomass‐burning emissions and associated haze layers over Amazonia, J. Geophys. Res. -Atmos., 93, 1509-1527, 1988.

Andreae, M. O., and Merlet, P.: Emission of trace gases and aerosols from biomass burning, Global biogeochem. cy., 15, 955-966, 2001.

Bonasoni, P., Laj, P., Marinoni, A., Sprenger, M., Angelini, F., Arduini, J., Bonafè, U., Calzolari, F., Colombo, T., Decesari, S., Di Biagio, C., di Sarra, A. G., Evangelisti, F., Duchi, R., Facchini, M. C., Fuzzi, S., Gobbi, G. P., Maione, M., Panday, A., Roccato, F., Sellegri, K., Venzac, H., Verza, G. P., Villani, P., Vuillermoz, E., and Cristofanelli, P.: Atmospheric Brown Clouds in the Himalayas: first two years of continuous observations at the Nepal Climate Observatory-Pyramid (5079 m), Atmos. Chem. Phys., 10, 7515-7531, 10.5194/acp-10-7515-2010, 2010.

Cachier, H., Liousse, C., Buat-Menard, P., and Gaudichet, A.: Particulate content of savanna fire emissions, J. Atmos. Chem., 22, 123-148, 1995.

Cao, J., Lee, S., Chow, J., Watson, J., Ho, K., Zhang, R., Jin, Z., Shen, Z., Chen, G., and Kang, Y.: Spatial and seasonal distributions of carbonaceous aerosols over China, J. Geophys. Res. -Atmos., 112, D22S11, doi:10.1029/2006JD008205, 2007.

Cao, J., Xu, B., He, J., Liu, X., Han, Y., Wang, G., and Zhu, C.: Concentrations, seasonal variations, and transport of carbonaceous aerosols at a remote Mountainous region in western China, Atmos. Environ., 43, 4444-4452, 2009.

Carrico, C. M., Bergin, M. H., Shrestha, A. B., Dibb, J. E., Gomes, L., and Harris, J. M.: The importance of carbon and mineral dust to seasonal aerosol properties in the Nepal Himalaya, Atmos. Environ., 37, 2811-2824, 2003.

Castro, L., Pio, C., Harrison, R. M., and Smith, D.: Carbonaceous aerosol in urban and rural European atmospheres: estimation of secondary organic carbon concentrations, Atmos. Environ., 33, 2771-2781, 1999.

Chen, X., Su, Z., Ma, Y., and Sun, F.: Analysis of Land-Atmosphere Interactions over the North Region of Mt. Qomolangma (Mt. Everest), Arct. Antarct. Alp. Res., 44, 412-422, 2012.

Chow, J. C., Watson, J. G., Chen, L. W. A., Chang, M. C. O., Robinson, N. F., Trimble, D., and Kohl, S.: The IMPROVE-A temperature protocol for thermal/optical carbon analysis: maintaining consistency with a long-term database, J. Air Waste Manage., 57, 1014-1023, 2007.

Claeys, M., Kourtchev, I., Pashynska, V., Vas, G., Vermeylen, R., Wang, W., Cafmeyer, J., Chi, X., Artaxo, P., and Andreae, M.: Polar organic marker compounds in atmospheric aerosols during the LBA-SMOCC 2002 biomass burning experiment in Rondônia, Brazil: sources and source processes, time series, diel variations and size distributions, Atmos. Chem. Phys., 10, 9319-9331, 2010.

Cong, Z., Kang, S., and Qin, D.: Seasonal features of aerosol particles recorded in snow from Mt. Qomolangma (Everest) and their environmental implications, J. Environ. Sci., 21, 914-919, 10.1016/s1001-0742(08)62361-x, 2009.

Cong, Z., Kang, S., Gao, S., Zhang, Y., Li, Q., and Kawamura, K.: Historical Trends of Atmospheric Black Carbon on Tibetan Plateau As Reconstructed from a 150-Year Lake Sediment Record, Environ. Sci. Technol., 47, 2579-2586, 2013.

480 Decesari, S., Facchini, M. C., Carbone, C., Giulianelli, L., Rinaldi, M., Finessi, E., Fuzzi, S., Marinoni, A.,
481 Cristofanelli, P., Duchi, R., Bonasoni, P., Vuillermoz, E., Cozic, J., Jaffrezo, J. L., and Laj, P.:
482 Chemical composition of PM10 and PM1 at the high-altitude Himalayan station Nepal
483 Climate Observatory-Pyramid (NCO-P) (5079 m a.s.l.), Atmos. Chem. Phys., 10,
484 4583-4596, 2010.
485 Draxler, R. R., and Rolph, G. D.: HYSPLIT (HYbrid Single-Particle Lagrangian Integrated Trajectory)
486 Model access via NOAA ARL READY Website, http://ready.arl.noaa.gov/HYSPLIT.php
487 NOAA Air Resources Laboratory, Silver Spring, MD., (last access: Jan. 7th, 2015), 2012.
488 Engling, G., Zhang, Y.-N., Chan, C.-Y., Sang, X.-F., Lin, M., Ho, K.-F., Li, Y.-S., Lin, C.-Y., and Lee, J. J.:
489 Characterization and sources of aerosol particles over the southeastern Tibetan Plateau
490 during the Southeast Asia biomass-burning season, Tellus B, 63, 117-128, 2011.
491 Fu, P., Kawamura, K., Okuzawa, K., Aggarwal, S. G., Wang, G., Kanaya, Y., and Wang, Z.: Organic
492 molecular compositions and temporal variations of summertime mountain aerosols over
493 Mt. Tai, North China Plain, J. Geophys. Res. -Atmos., 113, DOI: 10.1029/2008JD009900,
494 2008.
495 Fu, P., Kawamura, K., Chen, J., Li, J., Sun, Y., Liu, Y., Tachibana, E., Aggarwal, S., Okuzawa, K., and
496 Tanimoto, H.: Diurnal variations of organic molecular tracers and stable carbon isotopic
497 composition in atmospheric aerosols over Mt. Tai in the North China Plain: an influence
498 of biomass burning, Atmos. Chem. Phys., 12, 8359-8375, 2012.
499 Gobbi, G., Angelini, F., Bonasoni, P., Verza, G., Marinoni, A., and Barnaba, F.: Sunphotometry of the
500 2006–2007 aerosol optical/radiative properties at the Himalayan Nepal Climate
501 Observatory-Pyramid (5079 m asl), Atmos. Chem. Phys., 10, 11209-11221, 2010.
502 Hindman, E. E., and Upadhyay, B. P.: Air pollution transport in the Himalayas of Nepal and Tibet
503 during the 1995–1996 dry season, Atmos. Environ., 36, 727-739, 2002.
504 Kang, S., Xu, Y., You, Q., Flügel, W. A., Pepin, N., and Yao, T.: Review of climate and cryospheric
505 change in the Tibetan Plateau, Environ. Res. Lett., 5, 015101 doi:10.1088/1748-
506 9326/5/1/015101, 2010.
507 Kaspari, S., Schwikowski, M., Gysel, M., Flanner, M., Kang, S., Hou, S., and Mayewski, P.: Recent
508 increase in black carbon concentrations from a Mt. Everest ice core spanning 1860-2000
509 AD, Geophys. Res. Lett, 38, L04703, doi:04710.01029/02010GL046096, 2011.
510 Kopacz, M., Mauzerall, D. L., Wang, J., Leibensperger, E. M., Henze, D. K., and Singh, K.: Origin and
511 radiative forcing of black carbon transported to the Himalayas and Tibetan Plateau,
512 Atmos. Chem. Phys., 11, 2837-2852, 2011.
513 Kundu, S., Kawamura, K., Andreae, T. W., Hoffer, A., and Andreae, M. O.: Diurnal variation in the
514 water-soluble inorganic ions, organic carbon and isotopic compositions of total carbon
515 and nitrogen in biomass burning aerosols from the LBA-SMOCC campaign in Rondônia,
516 Brazil, J. Aerosol Sci., 41, 118-133, 2010.
517 Li, J., Pósfai, M., Hobbs, P. V., and Buseck, P. R.: Individual aerosol particles from biomass burning
518 in southern Africa: 2, Compositions and aging of inorganic particles, J. Geophys. Res.
519 -Atmos., 108, 8484, 10.1029/2002JD002310, 2003.
520 Li, J. J., Wang, G. H., Wang, X. M., Cao, J. J., Sun, T., Cheng, C. L., Meng, J. J., Hu, T. F., and Liu, S. X.:
521 Abundance, composition and source of atmospheric PM 2.5 at a remote site in the
522 Tibetan Plateau, China, Tellus B, 65, 2013.
523 Li, M., Ma, Y., and Zhong, L.: The turbulence characteristics of atmospheric surface layer on the

north slope of Mt. Everest region in the spring of 2005, J. Meteorol. Soc. Jpn., 90, 185-193, 2012.
Lu, Z., Streets, D. G., Zhang, Q., and Wang, S.: A novel back-trajectory analysis of the origin of black carbon transported to the Himalayas and Tibetan Plateau during 1996-2010, Geophys. Res. Lett., 39, L01809, doi:01810.01029/02011GL049903, 2012.
Lüthi, Z. L., Škerlak, B., Kim, S. W., Lauer, A., Mues, A., Rupakheti, M., and Kang, S.: Atmospheric brown clouds reach the Tibetan Plateau by crossing the Himalayas, Atmos. Chem. Phys. Discuss., 14, 28105-28146, 10.5194/acpd-14-28105-2014, 2014.
Ma, J., Tang, J., Li, S. M., and Jacobson, M. Z.: Size distributions of ionic aerosols measured at Waliguan Observatory: Implication for nitrate gas - to - particle transfer processes in the free troposphere, J. Geophys. Res. -Atmos., 108, 2003.
Ma, Y., Wang, Y., Zhong, L., Wu, R., Wang, S., and Li, M.: The Characteristics of Atmospheric Turbulence and Radiation Energy Transfer and the Structure of Atmospheric Boundary Layer over the Northern Slope Area of Himalaya, J. Meteorol. Soc. Jpn., 89A, 345-353, 2011.
Marinoni, A., Cristofanelli, P., Laj, P., Duchi, R., Calzolari, F., Decesari, S., Sellegri, K., Vuillermoz, E., Verza, G., and Villani, P.: Aerosol mass and black carbon concentrations, a two year record at NCO-P (5079 m, Southern Himalayas), Atmos. Chem. Phys., 10, 8551-8562, 2010.
Menon, S., Koch, D., Beig, G., Sahu, S., Fasullo, J., and Orlikowski, D.: Black carbon aerosols and the third polar ice cap, Atmos. Chem. Phys., 10, 4559-4571, 2010.
Ming, J., Zhang, D., Kang, S., and Tian, W.: Aerosol and fresh snow chemistry in the East Rongbuk Glacier on the northern slope of Mt. Qomolangma (Everest), J. Geophys. Res. -Atmos., 113, 10.1029/2008jd010430, 2008.
Ming, J., Xiao, C., Sun, J., Kang, S., and Bonasoni, P.: Carbonaceous particles in the atmosphere and precipitation of the Nam Co region, central Tibet, J. Environ. Sci., 22, 1748-1756, 2010.
Miyazaki, Y., Kawamura, K., and Sawano, M.: Size distributions and chemical characterization of water - soluble organic aerosols over the western North Pacific in summer, J. Geophys. Res. -Atmos., 115, DOI: 10.1029/2010JD014439, 2010.
Psichoudaki, M., and Pandis, S. N.: Atmospheric Aerosol Water-Soluble Organic Carbon Measurement: A Theoretical Analysis, Environ. Sci. Technol., 47, 9791-9798, 2013.
Qian, Y., Flanner, M., Leung, L., and Wang, W.: Sensitivity studies on the impacts of Tibetan Plateau snowpack pollution on the Asian hydrological cycle and monsoon climate, Atmos. Chem. Phys., 11, 1929-1948, 2011.
Qian, Y., Yasunari, T. J., Doherty, S. J., Flanner, M. G., Lau, W. K., Ming, J., Wang, H., Wang, M., Warren, S. G., and Zhang, R.: Light-absorbing particles in snow and ice: Measurement and modeling of climatic and hydrological impact, Adv. Atmos. Sci., 32, 64-91, 2015.
Qiu, J.: The third pole, Nature, 454, 393-396, 2008.
Ram, K., Sarin, M. M., and Hegde, P.: Long-term record of aerosol optical properties and chemical composition from a high-altitude site (Manora Peak) in Central Himalaya, Atmos. Chem. Phys., 10, 11791-11803, 2010.
Ramanathan, V., Chung, C., Kim, D., Bettge, T., Buja, L., Kiehl, J. T., Washington, W. M., Fu, Q., Sikka, D. R., and Wild, M.: Atmospheric brown clouds: Impacts on South Asian climate and hydrological cycle, Proc. Natl. Acad. Sci. U. S. A., 102, 5326-5333, 2005.
Ramanathan, V., and Carmichael, G.: Global and regional climate changes due to black carbon, Nat.

Geosci., 1, 221-227, 2008.
Simoneit, B. R., Schauer, J. J., Nolte, C., Oros, D. R., Elias, V. O., Fraser, M., Rogge, W., and Cass, G. R.: Levoglucosan, a tracer for cellulose in biomass burning and atmospheric particles, Atmos. Environ., 33, 173-182, 1999.
Stocker, T. F., Dahe, Q., and Plattner, G.-K.: Climate Change 2013: The Physical Science Basis, Working Group I Contribution to the Fifth Assessment Report of the Intergovernmental Panel on Climate Change. Summary for Policymakers (IPCC, 2013), 2013.
Stone, E. A., Schauer, J. J., Pradhan, B. B., Dangol, P. M., Habib, G., Venkataraman, C., and Ramanathan, V.: Characterization of emissions from South Asian biofuels and application to source apportionment of carbonaceous aerosol in the Himalayas, J. Geophys. Res. -Atmos., 115, doi:10.1029/2009JD011881, 2010.
Turpin, B. J., and Huntzicker, J. J.: Identification of secondary organic aerosol episodes and quantitation of primary and secondary organic aerosol concentrations during SCAQS, Atmos. Environ., 29, 3527-3544, 1995.
Vadrevu, K. P., Ellicott, E., Giglio, L., Badarinath, K. V. S., Vermote, E., Justice, C., and Lau, W. K. M.: Vegetation fires in the himalayan region – Aerosol load, black carbon emissions and smoke plume heights, Atmos. Environ., 47, 241-251, 2012.
Wan, X., Kang, S., Wang, Y., Xin, J., Liu, B., Guo, Y., Wen, T., Zhang, G., and Cong, Z.: Size distribution of carbonaceous aerosols at a high-altitude site on the central Tibetan Plateau (Nam Co Station, 4730ma. sl), Atmos. Res., 153, 155-164, 2015.
Wang, R., Tao, S., Balkanski, Y., Ciais, P., Boucher, O., Liu, J., Piao, S., Shen, H., Vuolo, M. R., and Valari, M.: Exposure to ambient black carbon derived from a unique inventory and high-resolution model, P. Natl. Acad. Sci. USA, 111, 2459-2463, 2014a.
Wang, X., Gong, P., Yao, T., and Jones, K. C.: Passive air sampling of organochlorine pesticides, polychlorinated biphenyls, and polybrominated diphenyl ethers across the Tibetan Plateau, Environ. Sci. Technol., 44, 2988-2993, 2010.
Wang, X., Xu, B., and Ming, J.: An overview of the studies on black carbon and mineral dust deposition in snow and ice cores in East Asia, J. Meteorol. Res., 28, 354-370, 2014b.
Watson, J. G., Chow, J. C., and Houck, J. E.: PM2.5 chemical source profiles for vehicle exhaust, vegetative burning, geological material, and coal burning in Northwestern Colorado during 1995, Chemosphere, 43, 1141-1151, 2001.
Wu, G., and Zhang, Y.: Tibetan Plateau forcing and the timing of the monsoon onset over South Asia and the South China Sea, Mon. Weather Rev., 126, 913-927, 1998.
Xia, X., Zong, X., Cong, Z., Chen, H., Kang, S., and Wang, P.: Baseline continental aerosol over the central Tibetan plateau and a case study of aerosol transport from South Asia, Atmos. Environ., 45, 7370-7378, 2011.
Xu, B., Cao, J., Hansen, J., Yao, T., Joswia, D. R., Wang, N., Wu, G., Wang, M., Zhao, H., Yang, W., Liu, X., and He, J.: Black soot and the survival of Tibetan glaciers, P. Natl. Acad. Sci. USA, 106, 22114-22118, 2009.
Xu, C., Ma, Y., Panday, A., Cong, Z., Yang, K., Zhu, Z., Wang, J., Amatya, P., and Zhao, L.: Similarities and differences of aerosol optical properties between southern and northern sides of the Himalayas, Atmos. Chem. Phys., 14, 3133-3149, 2014.
Yao, T., Thompson, L. G., Mosbrugger, V., Zhang, F., Ma, Y., Luo, T., Xu, B., Yang, X., Joswiak, D. R., Wang, W., Joswiak, M. E., Devkota, L. P., Tayal, S., Jilani, R., and Fayziev, R.: Third Pole

Environment (TPE), Environ. Dev., 3, 52-64, 2012.
Yasunari, T., Bonasoni, P., Laj, P., Fujita, K., Vuillermoz, E., Marinoni, A., Cristofanelli, P., Duchi, R., Tartari, G., and Lau, K. M.: Estimated impact of black carbon deposition during pre-monsoon season from Nepal Climate Observatory-Pyramid data and snow albedo changes over Himalayan glaciers, Atmos. Chem. Phys., 10, 6603-6615, 2010.
Zhao, Z., Cao, J., Shen, Z., Xu, B., Zhu, C., Chen, L. W. A., Su, X., Liu, S., Han, Y., and Wang, G.: Aerosol particles at a high - altitude site on the Southeast Tibetan Plateau, China: Implications for pollution transport from South Asia, J. Geophys. Res. -Atmos., 118, 11360-11375, 2013.
Zou, H., Zhou, L., Ma, S., Li, P., Wang, W., Li, A., Jia, J., and Gao, D.: Local wind system in the Rongbuk Valley on the northern slope of Mt. Everest, Geophys. Res. Lett., 35, DOI: 10.1029/2008GL033466, 2008.

628 **Table 1**. Seasonal average abundances (along with standard deviation) of OC, EC, WSOC

629 and water soluble ionic species (μg m^{-3}), as well as the ratios of OC/EC and WSOC/OC.

	Annual	Pre-monsoon	Monsoon	Post-monsoon	Winter
Number	50	13	11	13	13
Carbonaceous components					
OC	1.43±1.16	2.61±1.58	0.81±0.14	1.06±0.53	1.14±0.50
EC	0.25±0.22	0.44±0.31	0.10±0.06	0.19±0.07	0.26±0.12
OC/EC	6.69±6.33	6.63±4.05	10.58±11.95	5.56±2.03	5.18±3.58
WSOC	0.77±0.60	1.28±0.87	0.49±0.25	0.71±0.26	0.54±0.29
WSOC/OC	0.58±0.24	0.47±0.09	0.59±0.28	0.62±0.23	0.57±0.27
Levoglucosan	0.019±0.037	0.047±0.064	0.004±0.003	0.007±0.005	0.014±0.008
Water-soluble inorganic ions					
Cl^-	0.02±0.03	0.04±0.04	0.01±0.01	0.02±0.02	0.02±0.04
NO_3^-	0.20±0.27	0.51±0.37	0.06±0.04	0.08±0.04	0.12±0.07
SO_4^{2-}	0.43±0.54	1.06±0.66	0.09±0.09	0.18±0.07	0.32±0.24
Na^+	0.07±0.06	0.13±0.06	0.04±0.04	0.04±0.03	0.06±0.05
NH_4^+	0.03±0.09	0.10±0.16	BDL	BDL	0.00±0.01
K^+	0.02±0.05	0.06±0.07	BDL	BDL	0.00±0.02
Ca^{2+}	0.88±0.56	1.19±0.48	0.50±0.18	1.01±0.75	0.79±0.36
Mg^{2+}	0.04±0.02	0.06±0.02	0.02±0.01	0.05±0.01	0.04±0.01

630 BDL, Below Detection Limits (0.01 μg m^{-3} for cations and anions).

631

632

Table 2. Comparison of OC and EC concentrations (μg m^{-3}) and OC/EC ratios of aerosols from QOMS with other sites in the Himalayas and on the Tibetan Plateau.

Location	Description	Sample	Sampling period	OC	EC	OC/EC	Method	Reference
QOMS	Southern TP(4276 m)	TSP	Aug 2009 - Jul 2010	1.43±1.16	0.25±0.22	6.7 (1.91-43.8)	TOR	This study
Nam Co	Central TP (4730 m)	TSP	Jul 2006-Jan 2007	1.66±0.79	0.082±0.07	31.9±31.1	TOR	(Ming et al., 2010)
Muztagh Ata,	Northwest TP(4500 m)	TSP	Dec 2003-Feb 2005	0.48	0.055	10 (2.9-32.1)	TOR	(Cao et al., 2009)
Qinghai Lake	Northeast TP (3200 m)	PM2.5	Jul-Aug 2010	1.58±0.59	0.37±0.24	5.9(1.85-21.8)	TOR	(Li et al., 2013)
Lulang	Southeast TP(3360 m)	TSP	Jul 2008-July 2009	4.28±2.05	0.52±0.35	1.7-58.4	TOR	(Zhao et al., 2013)
Tengchong	Southeast TP(1640 m)	PM10	Apr-May 2004	5.8±4.4	1.5±1.0	2.63	TOR	(Engling et al., 2011)
Manora Peak, India	Himalayas (1950 m)	TSP	Feb 2005-Jul 2008	8.2±5.2	1.3±1.2	7.3±3.4	TOT	(Ram et al., 2010)
NCO-P, Nepal	Himalayas(5079 m)	PM10	Premonsoon 2006-2008	2.4	0.5	4.8	TOT	(Decesari et al., 2010)
			Monsoon	0.9	0.1	9		
			Postmonsoon	1.4	0.1	14		
			Dry season	1.2	0.1	12		
Langtang, Nepal	Himalayas (3920 m)	PM2.5	Jun –Sep 1999	0.75±0.69	0.15±0.16	5.0	TOT	(Carrico et al., 2003)
			Oct 1999-Jan 2000	1.81±1.25	0.52±0.48	3.48		
			Feb-May 2000	3.44±4.19	0.48±0.38	7.17		
Godavari, Nepal	S. Himalayas (1600 m)	PM2.5	2006	4.8±4.4	1.0±0.8	4.8	TOT	(Stone et al., 2010)

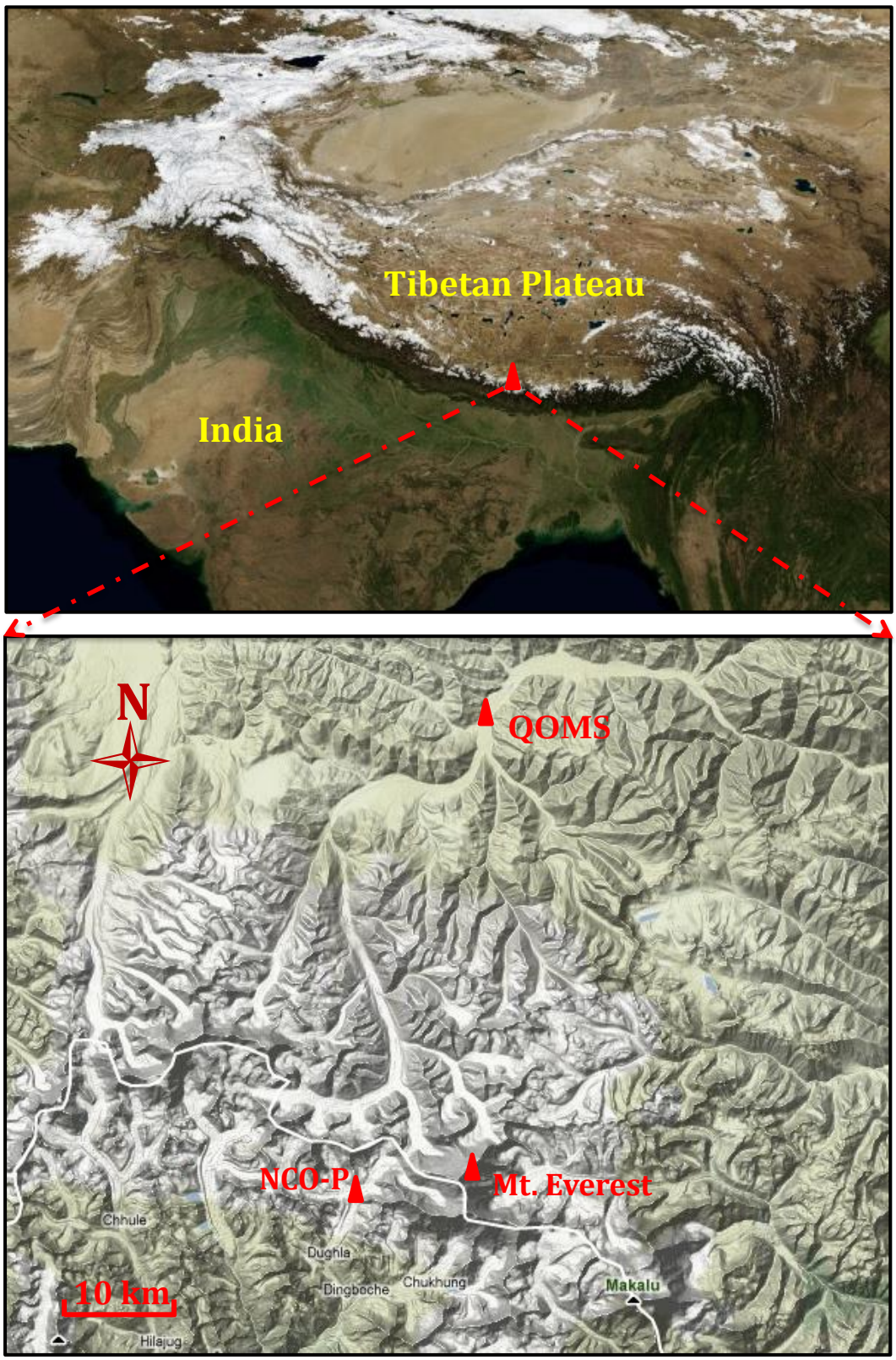

Fig. 1 Location of the sampling site (QOMS, 4276 m a.s.l.) at the south rim of the Tibetan Plateau, with the NCO-P (5079 m a.s.l.) and the summit of Mt. Everest (8844 m a.s.l.).

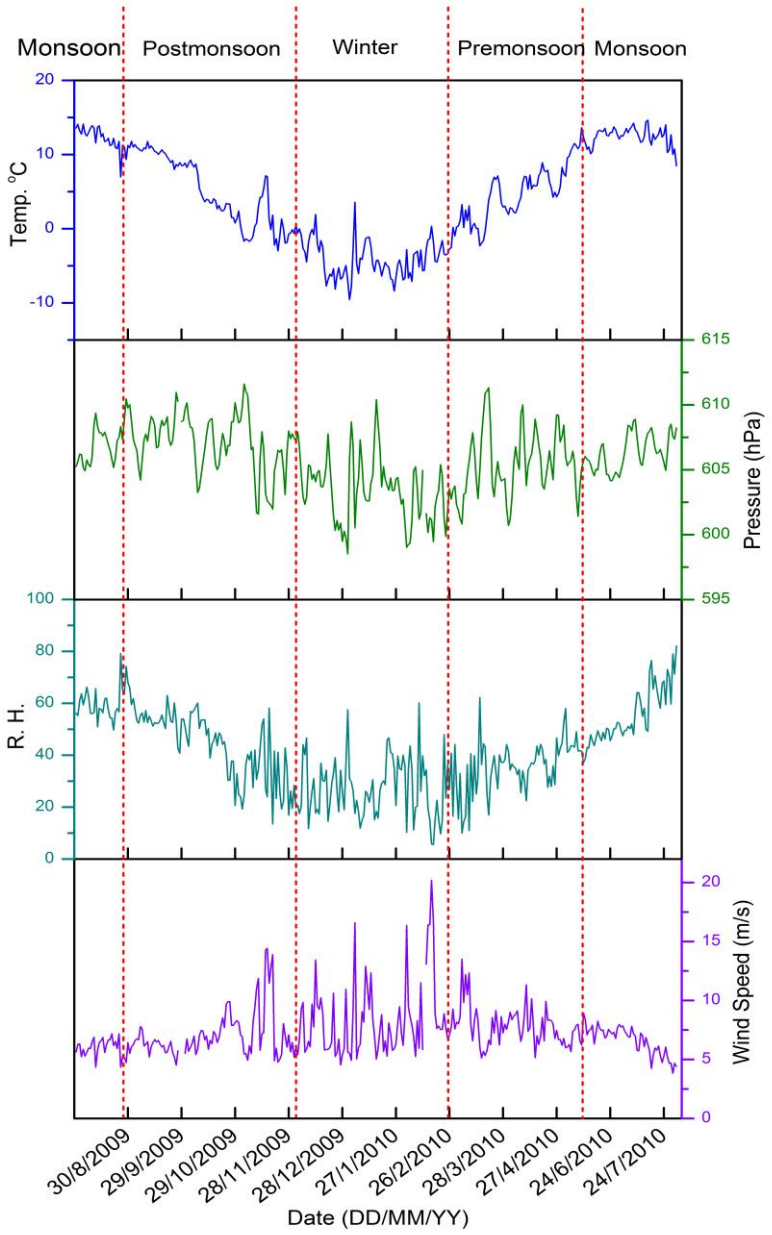

Fig. 2. Time-series of ambient temperature, atmospheric pressure, relative humidity and wind speed at QOMS from August 2009 to July 2010.

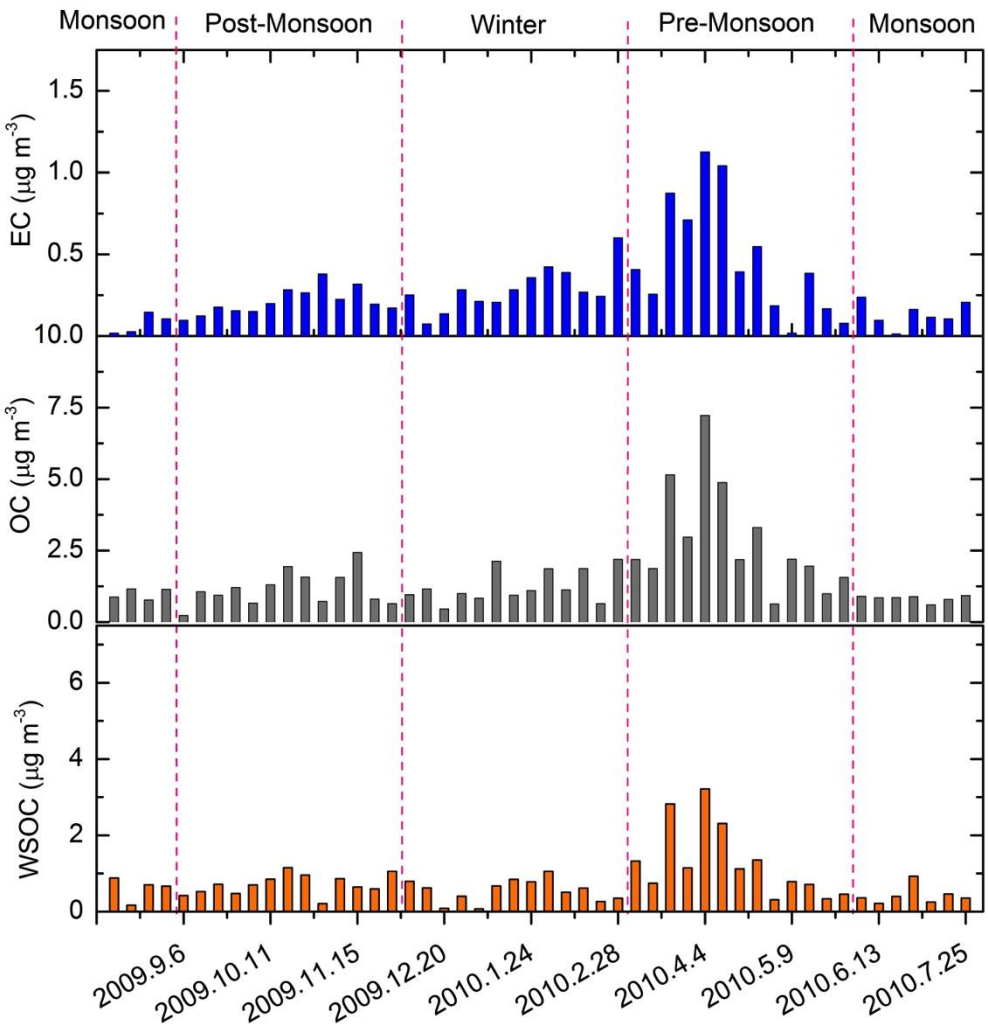

Fig. 3. Temporal variations (weekly) of OC, EC and WSOC at the QOMS site from August 2009 to July 2010.

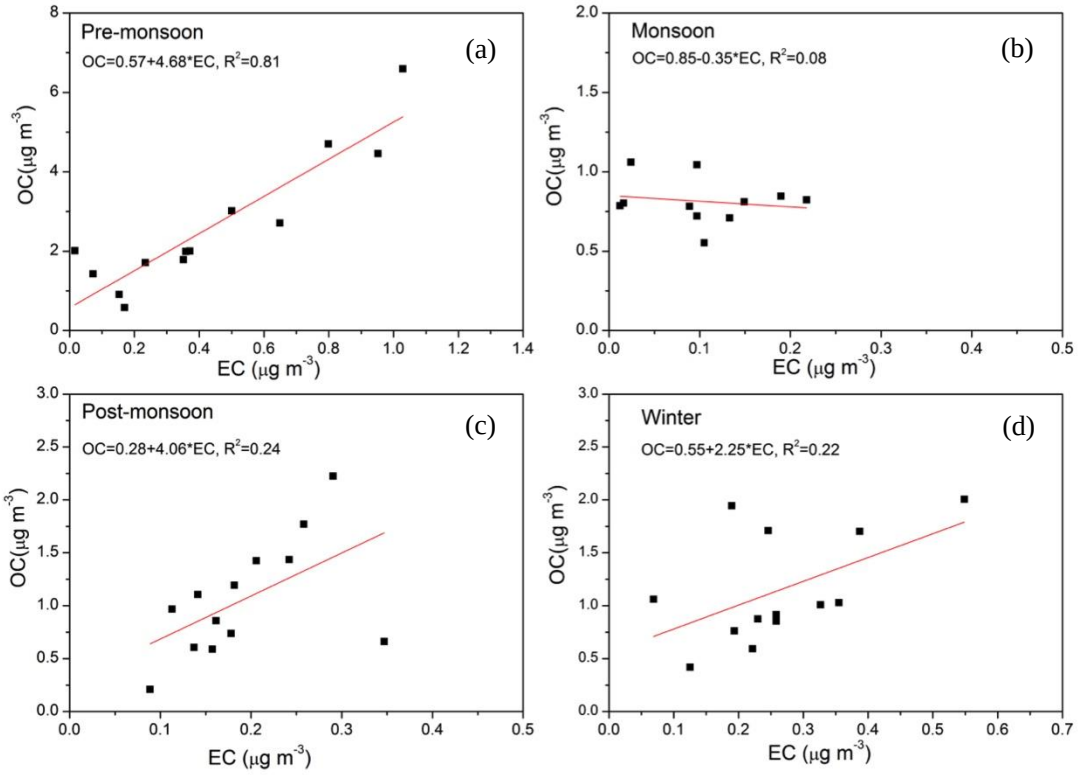

Fig. 4. Relationship between OC and EC in aerosols of different seasons at QOMS.

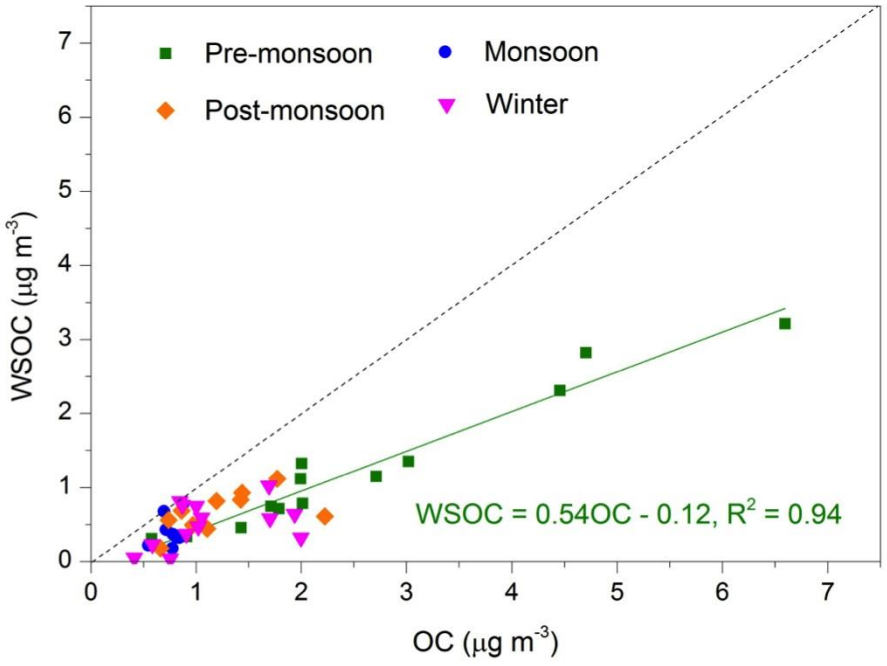

Fig. 5. Relationship between WSOC and OC in aerosols from QOMS.

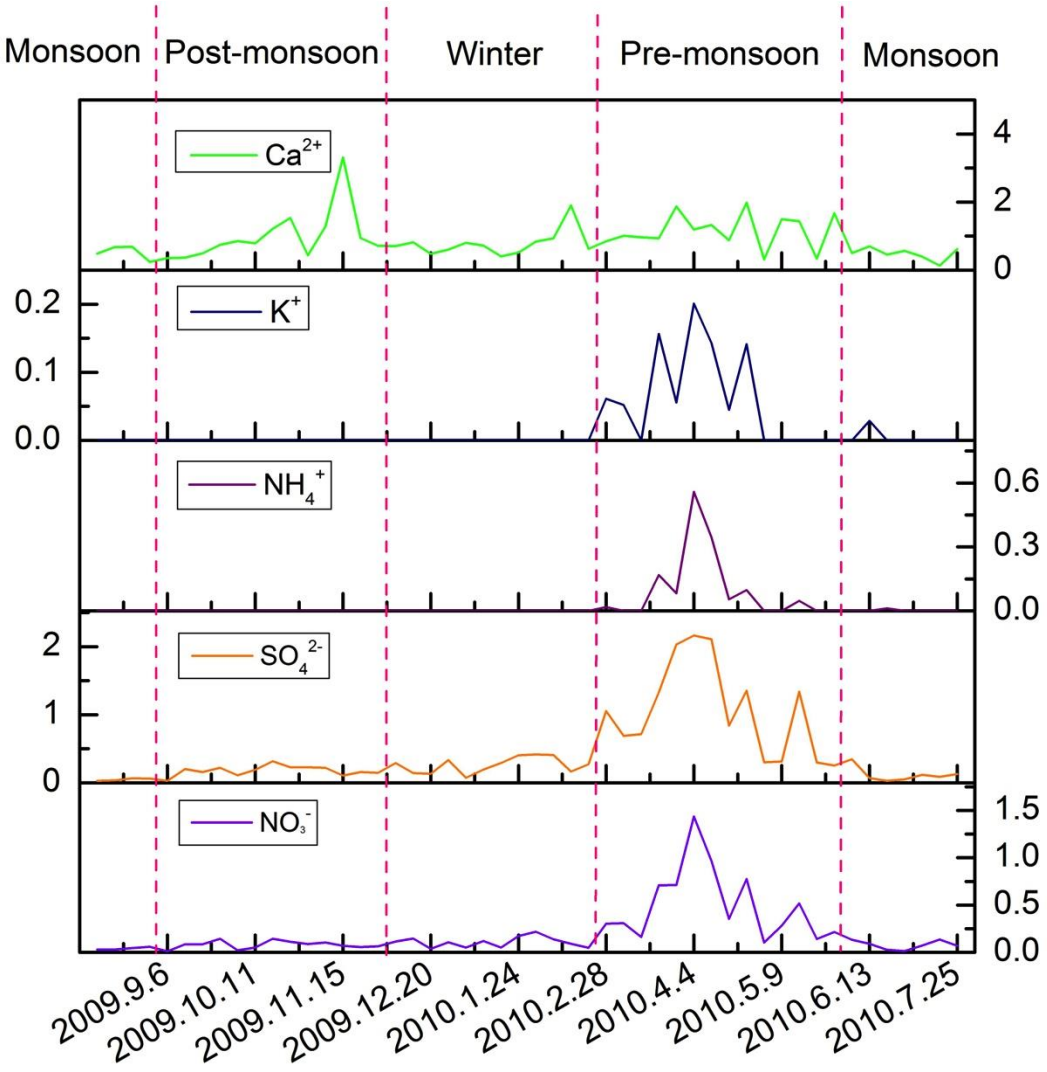

Fig. 6. Temperal variations (weekly) of water-soluble ionic species (Ca^{2+}, K^{+}, NH_4^{+}, SO_4^{2-} and NO_3^{-}) in aerosols collected at QOMS (Units: μg m^{-3}).

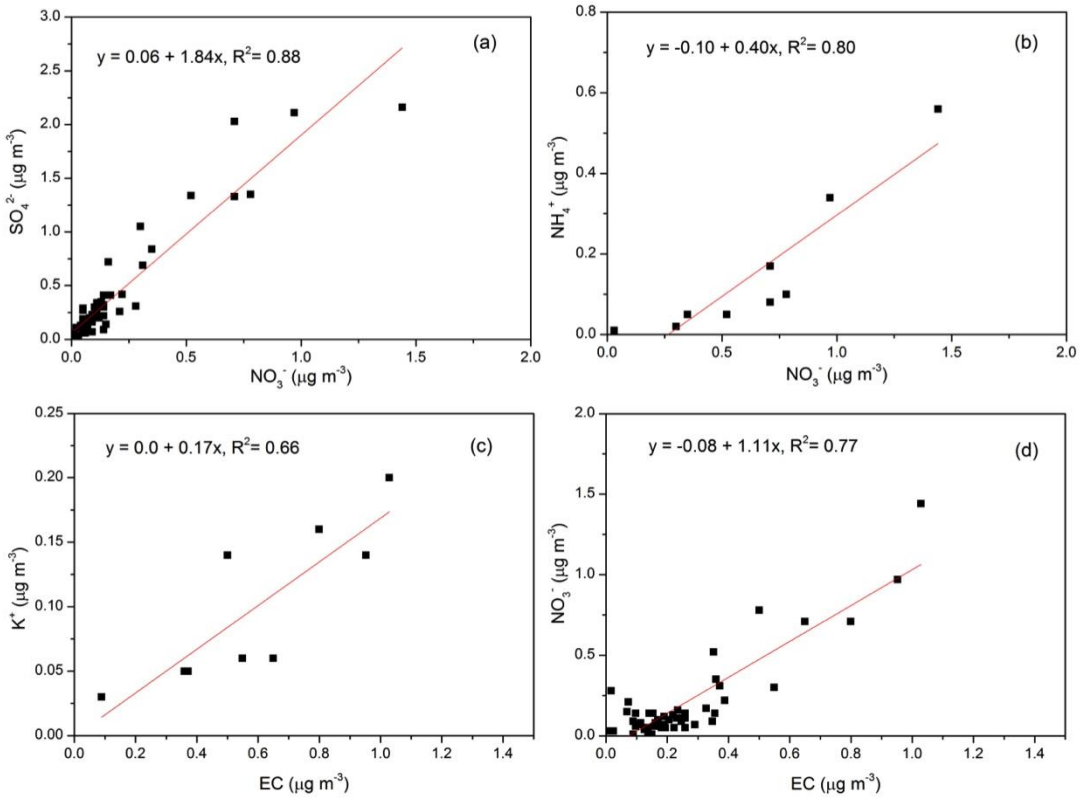

Fig. 7. Correlations between various chemical components. (a) SO_4^{2-} and NO_3^-, (b) NH_4^+ and NO_3^-, (c) K^+ and EC, (d) NO_3^- and EC.

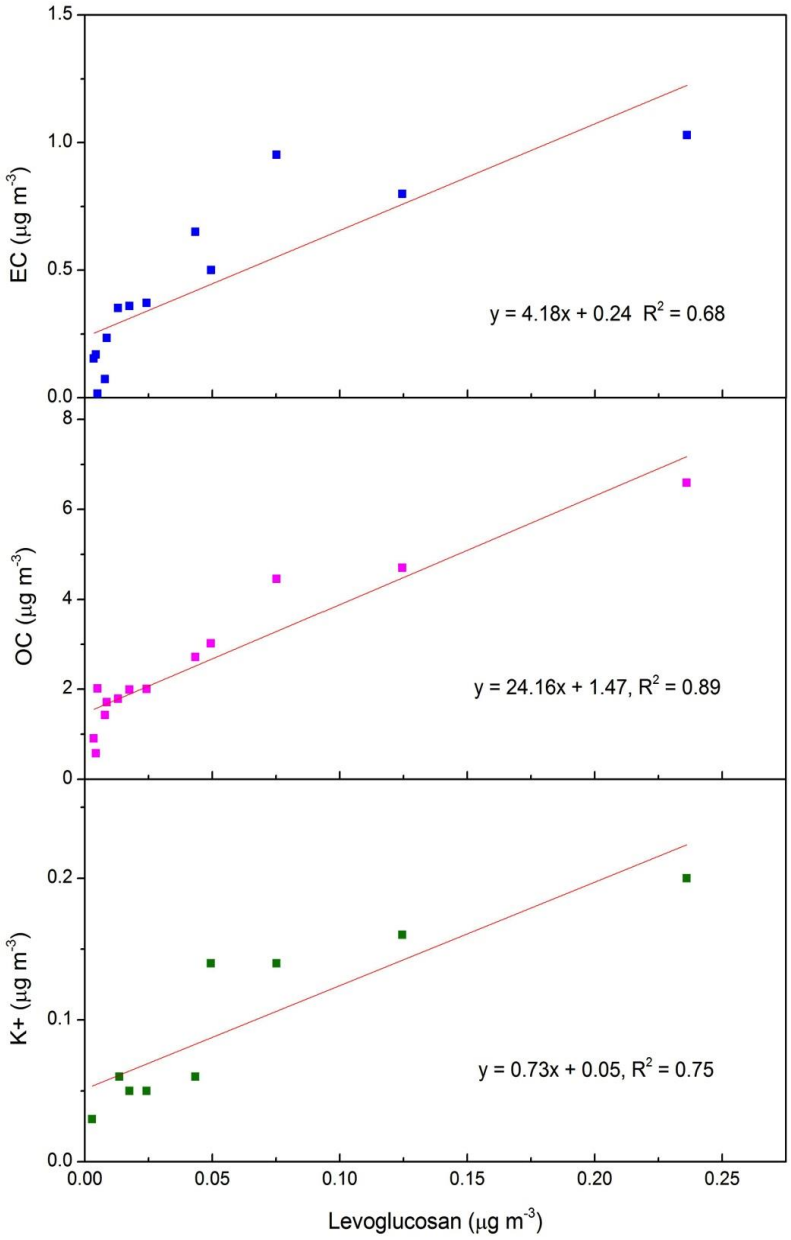

Fig. 8. The relationship between EC, OC, K^+ and levoglucosan in aerosols at QOMS during the pre-monsoon season, 2010.

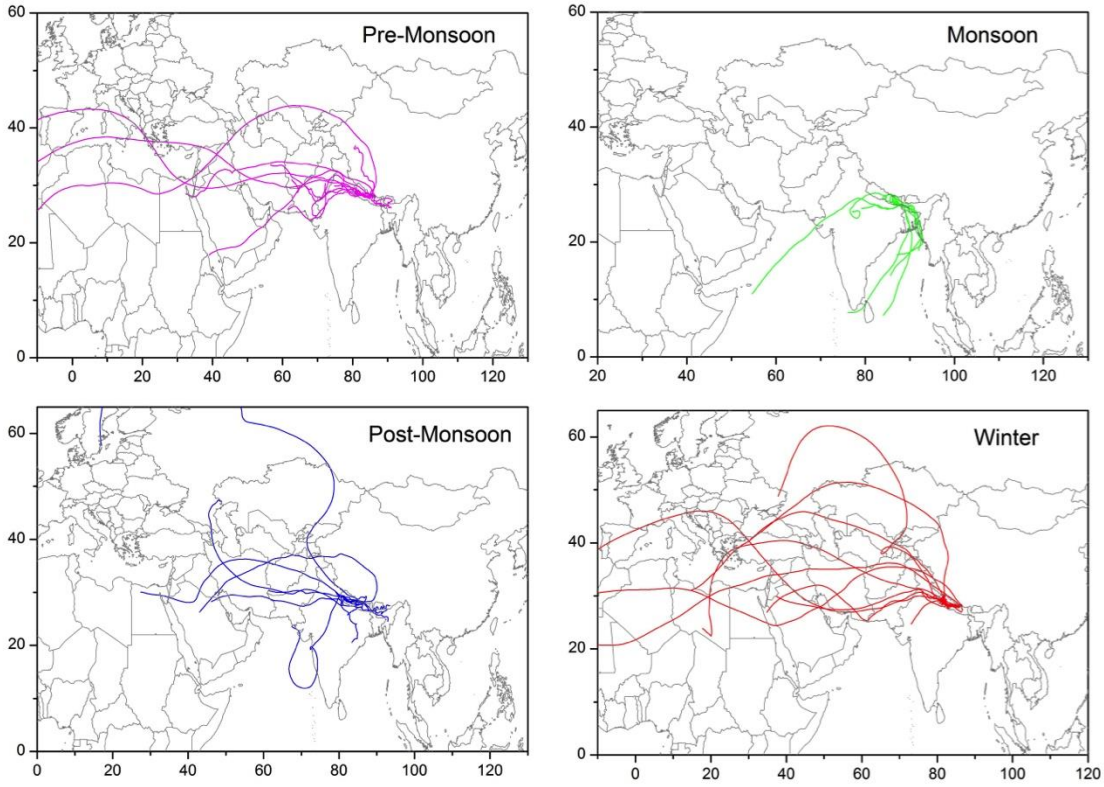

Fig. 9. Seven-day backward trajectories at QOMS on each sampling day during different seasons.

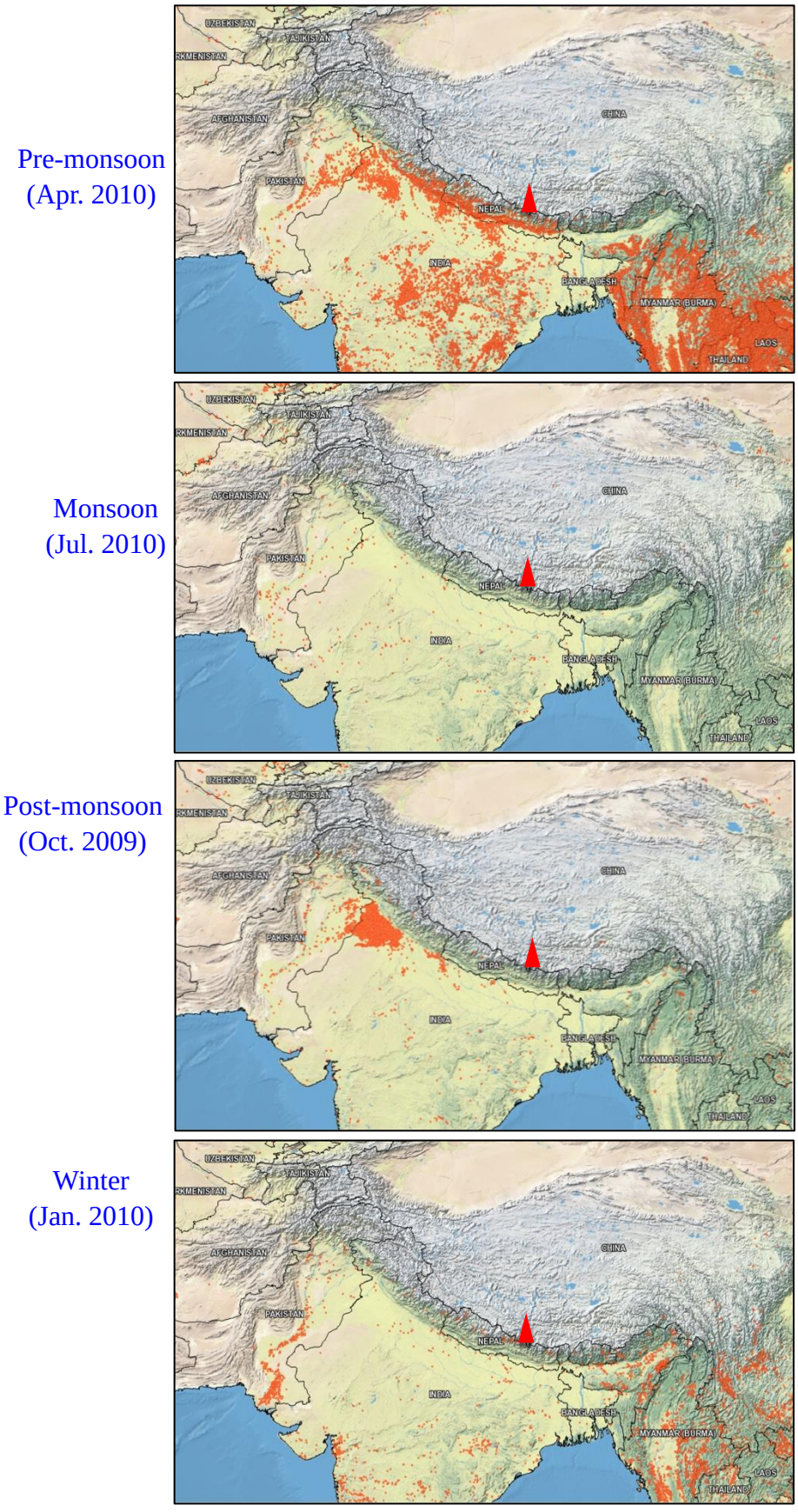

Fig. 10. The spatial distribution of fire spots observed by MODIS in different seasons (Aug. 2009 to Jul. 2010) (https://firms.modaps.eosdis.nasa.gov/firemap/).

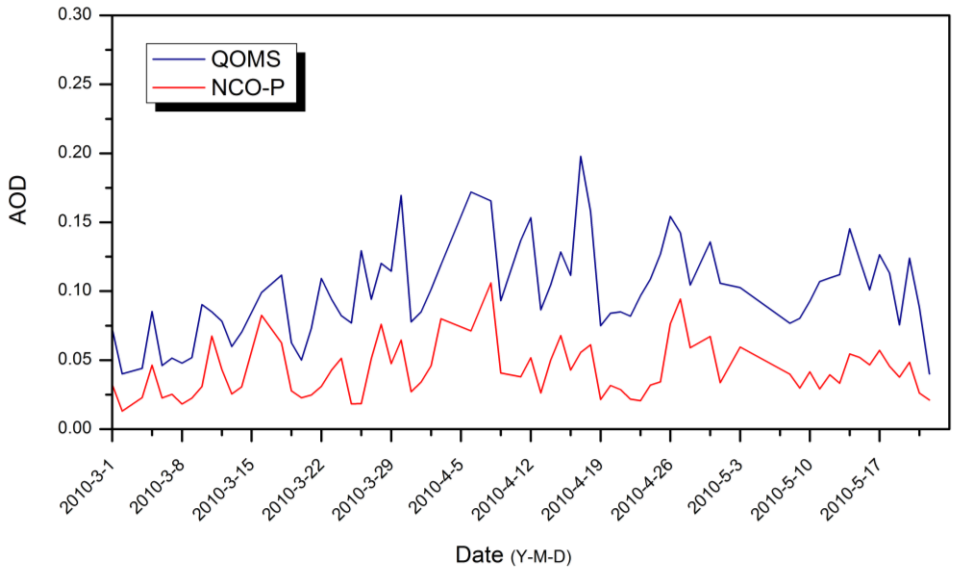

Fig. 11. The temporal variations of the daily aerosol optical depth (AOD, 500nm) at QOMS and NCO-P during the pre-monsoon season, 2010 (n=70).